Multi-Objective Bacterial Foraging Optimization Algorithm Based on Parallel Cell Entropy for Aluminum Electrolysis Production Process

Jun Yi, Di Huang, Siyao Fu, *Member, IEEE*, Haibo He, *Senior Member, IEEE*, and Taifu Li

***Abstract*—Environment-friendly aluminum electrolysis production process has long been a challenging industrial issue due to its built-in difficulty in optimizing numerous highly coupled and nonlinear parameters. This paper presents a multi-objective bacterial foraging optimization (MOBFO) algorithm to find optimal solutions that maximize the current efficiency and minimize the energy consumption and the production of perfluorocarbons (PFCs). Our method can be viewed as an enhanced version of the bacterial foraging optimization (BFO) in solving multi-objective optimization (MOO) problems (MOPs). We first propose a task-oriented optimization framework and model, and then parallel cell entropy and its difference are introduced to evaluate the evolutionary status of the Pareto solutions in a new objective space called parallel cell coordinate system (PCCS). In particular, the Pareto-archived evolution approach (PAEA) and the adaptive foraging strategy (AFS) are applied to balance the convergence and diversity of the Pareto front in the optimization procedure. Compared with traditional approaches, MOBFO not only increases speed of convergence toward the Pareto front, but also improves the diversity of the obtained solutions. Extensive experiment results on numerous benchmark problems and real-world aluminum electrolysis production process validated our proposed method's effectiveness.**

***Index Terms*—Aluminum electrolysis production, bacterial foraging, entropy, multi-objective optimization (MOO), parallel cell, Pareto front.**

Manuscript received May 4, 2015; revised October 12, 2015; accepted November 15, 2015. Date of publication December 22, 2015; date of current version March 8, 2016. This work was supported in part by the National Science Foundation (NSF) under Grant ECCS 1053717, in part by the National Natural Science Foundation of China under Grant 51374268, Grant 51375520, Grant 51404051, and Grant 61503050, in part by the Application Development Major Projects of Chongqing under Grant cstc2013yykfC0034, in part by the Training Plan of Science and Technology Talent of Chongqing under Grant cstc2013kjrc-qnrc40008, in part by the Program for Innovation Team Building at Institutions of Higher Education under Grant KJTD201324, and in part by the Achievement Transfer Program of Institutions of Higher Education in Chongqing under Grant KJZH14218.

J. Yi, D. Huang, and T. Li are with the College of Electronic and Information Engineering, Chongqing University of Science and Technology, Chongqing 401331, China (e-mail: laoyifrcq@163.com; hlhuangdi@qq.com; litaifuemail@qq.com).

S. Fu is with the Department of Computer Science, University of Massachusetts Boston, Boston, MA 02125 USA (e-mail: siyao.fu@umb.edu).

H. He is with the Department of Electrical, Computer, and Biomedical Engineering, University of Rhode Island, Kingston, RI 02881 USA (e-mail: he@ele.uri.edu).

Color versions of one or more of the figures in this paper are available online at http://ieeexplore.ieee.org.

Digital Object Identifier 10.1109/TIE.2015.2510977

Nomenclature

p	Dimension of the search space.
S	Number of bacteria.
N_c	Number of chemotaxis steps.
N_{ed}	Number of elimination-dispersal steps.
P_{ed}	Probability of elimination-dispersal steps.
m	Number of objective functions.
t	Iteration time.
$T_{\max}$	Maximum time of iterations.

I. Introduction

THE Hall–Héroult process is the standard method for large-scale production of metallic aluminum [1]. The ultimate goal of the aluminum industry is to maximize productivity and efficiency with reduced energy requirements and costs. However, this goal is difficult to achieve because uncertainty and discontinuity measurement of parameters inevitably exists due to complex physical and chemical reactions and interference of various external conditions and manual operation [2]. In recent years, some of the promising technologies, such as allotype cathode [3] and perforated anode [4], have been applied to save energy. Fig. 1 shows a sketch of the equipment combined with application of two new technologies. In such cases, the system becomes more inefficient because it becomes very sensitive to uncertainties from system disturbance, state change, and its interaction, especially when the cell voltage is reduced to a certain extent. In fact, application of them, to a certain extent, exacerbate the problem. Therefore, the maximum of current efficiency and minimum of energy consumption as the multi-objective optimization (MOO) have become essential, yet challenging, and rarely touched in the aluminum industry control community [5], [6].

Many existing techniques have been proposed to deal with MOO problems (MOPs) [7]–[9]. For instance, Zhang and Li propose a multi-objective evolutionary algorithm based on decomposition (MOEA/D) [10], which decomposes a MOP into a number of different subproblems with single objective and uses a population-based method to optimize it. Zizler and Thiele attempt to strengthen the Pareto evolutionary algorithm (SPEA) [11] to find the Pareto-optimal set. Furthermore, they propose the SPEA2 method [12], which incorporates a fine-grained fitness assignment strategy to yield promising

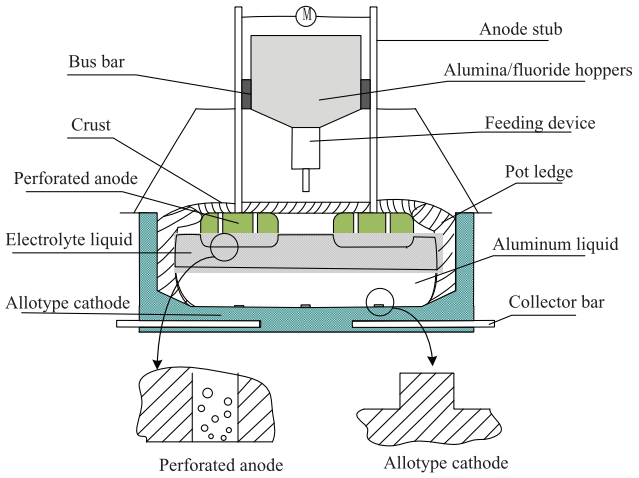

Fig. 1. Alumina reduction cell combined with two energy-saving technologies; specifically, allotype cathode can reduce the velocity of liquid metal and the surface oscillation of liquid meta, and perforated anode can diminish the gas bubbles, by which the carbon dioxide gas at the bottom of the anode can be discharged through designed holes.

results. Knowles and Corne developed the Pareto-archived evolution strategy (PAES) [13], the Pareto envelope-based selection algorithm (PESA) [14], and its modification PESA-II [15], which employ a new selection method. Coello and Pulido propose a micro-genetic algorithm (micro-GA) [16], which is an improved GA with a small population and a reinitialization process. Deb *et al.* propose the nondominated sorting GA II (NSGA-II) [17] to find much better spread of solutions and convergence. In addition to these classical multi-objective algorithms, new evolutionary paradigm and swarm intelligence methods have recently been introduced [18]–[21]. Coello *et al.* introduce a proposal for the multiple-objective particle swarm optimization (MOPSO) [22]. The nondominated neighbor immune algorithm (NNIA) [23] uses an immune-inspired operator, two heuristic search operators, and elitism to strengthen searching for the Pareto frontier in sparse areas. Zhang and Zhou propose a regularity model-based multi-objective estimation of distribution algorithm (RM-MEDA) [24] by inducing local principal component analysis (PCA) algorithm under mild conditions to build a probability distribution model. In fact, there are also many other heuristics reported [25]–[27].

Unfortunately, only a few of the proposed MOO algorithms have addressed the problem of uncertainty and discontinuity of parameters of the aluminum electrolysis production process. For instance, Guo *et al.* propose an improved hybrid differential evolution algorithm to adjust the Cryolite ratio, electrolytic temperature, and polar distance timely under different conditions [28], [29]. However, taking the minimum of the aluminum cell voltage as the objective function is unreasonable, and it is difficult to directly measure some selected decision-making parameters. The method is hardly able to obtain a set of precise Pareto solutions for real-world application.

In the past few years, a new swarm optimization algorithm, which is named as bacterial foraging optimization (BFO) algorithm [30], [31] and inspired by swarming and social foraging behaviors of *Escherichia coli* bacteria, has been proposed to solve a single-objective problem. BFO shows a superior optimized performance and excellent searching ability in solutions space because of its unique operations such as chemotaxis, swarming, elimination, and dispersal. To our knowledge, optimization algorithm based on BFO for MOPs is rarely reported in published work except for the multi-objective BFO (MBFO). However, MBFO does not contribute in improving the convergence when extending BFO. As we all know, the computation cost of optimization would be very important for industry processes such as the aluminum electrolysis production process. To cope with these problems, the MOBFO algorithm is presented in this work. Through deep analysis of mechanism of the aluminum production process, three objectives can be obtained. Parallel cell entropy and its difference are, then, introduced to evaluate diversity and convergence of the approximate Pareto front. Furthermore, two significant methods, the Pareto-archived evolution approach (PAEA) and the adaptive foraging strategy (AFS), have been proposed to improve the BFO algorithm in solving MOO problems. Experiment results are carried out on the benchmark problems and real case to verify the effectiveness of proposed method.

Compared with the state-of-the-art methods in the field, the advantages of the proposed algorithm are as follows.

1) *Task-oriented.* We propose a specialized MOO model in a new optimization framework for the aluminum production process.
2) *Simple and efficient.* We use a target spatial transform method to map the Cartesian coordinate system to the two-dimensional grid for performance evaluation of the Pareto front.
3) A delicate balance between convergence and divergence for the population. In particular, we use parallel cell entropy and its difference to evaluate the evolution status, and to further adjust the chemotaxis step size and update archive adaptively.
4) We further modify and extend the BFO method for MOPs.

This paper is organized as follows. In Section II, an MOO model with nonlinear equality and inequality constraints is formulated. In Section III, a brief introduction of the BFO algorithm is presented, and then the MOBFO algorithm is extended into the domain of MOO. Computational experiments are presented to study the performances of the proposed algorithms in Section IV. Finally, the conclusion is given in Section V.

II. Modeling and Analysis for Aluminum Production Process

A. Optimization Framework

With comprehensive application of data-driven techniques, the framework based on these techniques is attracting more and more attention both from industrial and academic domains [32]–[34]. In our work, the proposed MOO framework consisted of three main steps as shown in Fig. 2. The first one is the nonlinear feature selection method based on kernel PCA (KPCA) in our previous work [35]. Decision parameters $(x'_1, x'_2, x'_3, \ldots, x'_m)$ have to be selected to develop a precise model of the multi-objective function by calculating the

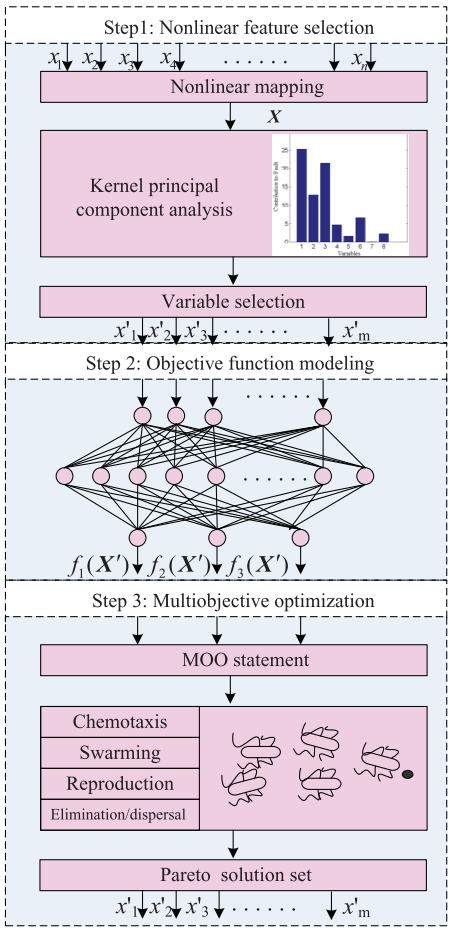

Fig. 2. Overview of the MOO framework. It is consisted of three main steps, and the third step is the main contribution of this paper.

cumulative contribution ratio for each parameter, which include the cell current I, the blanking times t_{NB}, the molecular ratio r_m, the bath temperature T_b, the cell voltage U, the amount of aluminum q', the height of the metal level h_m, and the electrolyte level h_e. The second step of the proposed framework leads to obtaining the optimum of the ith objective function $f_i(X')$ under multiphasic constraints by nonlinear modeling method such as artificial neural networks. The third step is the MOBFO, the main contribution of our work, which leads to optimization of the Pareto solution set to minimize the energy consumption and the perfluorocarbons (PFCs) emission and to maximize the current efficiency.

B. Process Analysis

There is a wide range of complex electrochemical reactions in the Hall–Héroult process; therefore, the control system must follow two basic laws: 1) material balance and 2) thermal balance, to maximize productivity and efficiency with reduced energy requirements. The dynamic change of the concentration of the electrolyte greatly influences the properties of the overall cell mode. Two balance models can be constructed by taking operating current, bath temperature, alumina, and sodium fluoride into account.

To simplify the material balance model, the concentration of alumina c can be expressed as equality constraints as shown in the following equation:

$$c = c_0 \left[1 - \exp\left(\frac{kA}{V} \cdot t_d\right)\right] \tag{1}$$

where c_0 is the alumina concentration at saturation, and k, A, V, and t_d are the dissolution constant of alumina, the dissolution area of alumina, the dissolution volume of alumina, and the dissolution period, respectively.

Conservation of energy should be considered, which reveals the principle of energy transfer through heat and mechanical work according to the first law of thermodynamics. The thermal balance model equation is

$$I\left(U - U_{\Delta H^0}\right) - h_b = 0 \tag{2}$$

where h_b, I, U, and $U_{\Delta H^0}$ represent the heat loss, the operating current, the cell voltage drop, and the minimum voltage required for the electrolysis of alumina, respectively. An aluminum cell is in thermal balance, only when (2) is true.

C. Optimization Objective Function

According to Faraday's law of electrolysis, the current efficiency CE is the ratio of the actual quantity of aluminum-produced q' to the theoretical quantity q. This can be defined as follows:

$$\mathrm{CE} = \frac{q'}{q} \times 100\%. \tag{3}$$

The current efficiency should be as high as possible. Taking the cell's design and other parameters, X', including the bath temperature, the cell voltage, the Cryolite ratio, and the interpolar distance into account, the maximum current efficiency is given by

$$\min \quad f_1(X') = 1 - \mathrm{CE}\left(I, t_{\mathrm{NB}}, r_m, T_b, U, q', h_m, h_e\right). \tag{4}$$

Energy consumption W is usually expressed by the consumed direct current (kilowatt hour) of the produced aluminum per ton under the given period t and the cell current I conditions. This can be expressed as

$$W = \frac{IUt \cdot 10^{-3}}{0.3356It \cdot \mathrm{CE} \cdot 10^{-6}} = 2980 \times \frac{U}{\mathrm{CE}}. \tag{5}$$

It can be observed from (5) that the energy consumption is proportional to the cell voltage. Some researches proposed optimization objective of the minimum of the cell voltage and considered that the cell voltage should be held as low as possible [28], [29]. Although energy consumption would be reduced when the cell voltage is decreased by shortening the interpolar distance, it would increase when the cell voltage is lower than the threshold limit. Therefore, the cell voltage should not be

a minimum objective but should be held within proper limits. Minimizing energy consumption can be expressed as

$$\min \quad f_2(X') = W(I, t_{\mathrm{NB}}, r_m, T_b, U, q', h_m, h_e). \tag{6}$$

The anode effect is an abnormal operating condition during the aluminum electrolytic process. When the anode effect occurs, large amounts of PFCs such as tetrafluoromethane CF_4 and hexafluoroethane C_2F_6 are produced besides decreasing both lifetime of the cell and the energy efficiency. The studies carried out in [36] have shown that the greenhouse effects of CF_4 and C_2F_6 are 6500 and 9200 times higher than that of CO_2, respectively. The generation of CF_4 is associated with the current by Faraday's law of electrolysis. Therefore, the production of CF_4 can be calculated using [37]

$$V_{\mathrm{CF_4}} = 1.698(P/\mathrm{CE}) \cdot F_{\mathrm{AE}} \cdot D_{\mathrm{AE}} \tag{7}$$

where P is the emission percentage of CF_4 and the anode gas during anode effect, and F_{AE} and D_{AE} represent the frequency and duration of the generated anode effect, respectively.

In (7), P depends on different operational parameters, which are influenced by cell design and operating procedures. Furthermore, the C_2F_6 emissions can be calculated to account for ten percent of the total CF_4 emissions in various calculation methods. CF_4 emissions represent periodically produced PFC from the Hall–Heroult process.

Minimizing the production of CF_4 can be given by

$$\min \quad f_3(X') = V_{\mathrm{CF_4}}(I, t_{\mathrm{NB}}, r_m, T_b, U, q', h_m, h_e). \tag{8}$$

In summary, the formulas of the multiple-objective functions can be given as follows:

$$\min \quad J(X') = [f_1(X'), f_2(X'), f_3(X')]^T. \tag{9}$$

To satisfy the requirements of the aluminum electrolytic process, in the case of 170KA series of aluminum reduction cell, we also define a series of equality and inequality constraints.

1) Equality Constraints: Decision parameters must also be subjected to (1)–(3), (5), and (7).

2) Inequality Constraints: Decision parameters must be satisfied; the threshold limits in real applications are as follows: $1660 \le I \le 1710$ A, $610 \le t_{\mathrm{NB}} \le 770$, $2.35 \le r_m \le 2.55\%$, $930 \le T_b \le 970$ °C, $3600 \le U \le 3750$ mV, $16 \le h_m \le 21$ cm, and $14 \le h_e \le 18$ cm.

III. Multi-Objective Approach

In this section, the parallel cell entropy and its difference, which characterize the diversity and convergence of the Pareto front, can be obtained by transforming the Cartesian coordinate into parallel cell coordinate system (PCCS) [38], [39].

A. Overview of the BFO Algorithms

In the BFO algorithm, individuals and populations of *Escherichia coli* can find favorable food resource in three operators according to the law of evolution of "the survival of the fittest": 1) chemotaxis; 2) reproduction; and 3) elimination-dispersal. During the past decades, BFO has been applied successfully in machine learning, optimal control, and transmission loss reduction [40], [41] due to its excellent local and global search properties. However, several challenges, such as storing and updating the Pareto set and selecting the global best solution, occur when extending the BFO algorithm for MOO problems.

B. Parallel Cell Entropy

PCCS [39] is a widely used method in analyzing multivariate data and visualizing high-dimensional geometry. The parallel coordinates have certain geometrical properties that can map high-dimensional Pareto front onto two-dimensional space to better evaluate the convergence and distribution of optimal solutions. The mapping formula can be expressed as follows:

$$L_{n,m} = \left\lceil \eta \frac{f_{n,m} - f_m^{\min}}{f_m^{\max} - f_m^{\min}} \right\rceil \tag{10}$$

where n is nondominated solutions with $n = 1, 2, \ldots, N$, m is optimal objects with $m = 1, 2, \ldots, M$, N is the number of nondominated solutions, and M is the number of objects. $L_{n,m}$ is the integer value by rounding up in two-dimensional space, $f_{n,m}$ is the mth objective value of the nth nondominated solution, $f_m^{\min}$ and $f_m^{\max}$ are the minimum and the maximum values of $f_{n,m}$, respectively, and η is the objective dimension split coefficient. Simultaneously, we also define the distance of the parallel cell (DPC (P_i, P_j)), which is a measure of how close an individual P_i is to its neighbors P_j. DPC (P_i, P_j) is calculated by

$$\mathrm{DPC}(P_i, P_j) = \begin{cases} \sum_{m=1}^{M} |L_{i,m} - L_{j,m}|, & \text{if } \exists m, L_{i,m} \neq L_{j,m} \\ 0.5, & \text{otherwise.} \end{cases} \tag{11}$$

Note that the parallel cell distance should be invariants if P_i and P_j share the same distribution of cell. The density of the solution is given as

$$D(P_i) = \sum_{j=1}^{N} \frac{1}{\mathrm{DPC}(P_i, P_j)^2}. \tag{12}$$

The parallel cell entropy $E(t)$, which was inspired by the entropy as a measure of uncertainty, is defined to evaluate the distribution of the Pareto optimal front in PCCS as shown by

$$E(t) = -\sum_{n=1}^{N} \sum_{m=1}^{M} \frac{TA_{n,m}(t)}{NM} \log \frac{TA_{n,m}(t)}{NM} \tag{13}$$

where $\mathrm{TA}_{n,m}(t)$ is the total amount of transformed Pareto fronts at the tth generation onto the nth row and the mth column cell. Furthermore, we give the definition of the differential entropy as follows:

$$\Delta E(t) = E(t) - E(t-1). \tag{14}$$

Algorithm 1. Pareto-archived evolution approach

Input: archive A, candidate solution m
Output: updated archive A'
if $A = \emptyset$ **then**
  $A' \leftarrow m$
else
  if m is dominated by a_i, and $\forall a_i \in A$ **then**
    m is rejected.
  else
    $A = A \,|\{a_i\}$
    if $A \neq \emptyset$ **then**
      $A' = A \cup \{m\}$
    else
      $B = A \cup \{m\}$, $\forall b_i \in B$, calculate $D(b_i)$.
      select $b_{\max}$.
      if $m = b_{\max}$ **then**
        m is rejected.
      else
        $A' = B \,|\{b_i\} \cup \{m\}$
      end if
    end if
  end if
end if

The cell coordinate components will be redistributed when the Pareto front changes; this will lead to further change in the parallel cell entropy $E(t)$. It is desired that the differential entropy $\Delta E(t)$ is variable to evaluate the change of $E(t)$ between the tth generation and the $(t-1)$th one.

C. Pareto-Archived Evolution Approach

To maintain the diversity of the Pareto front, an archive of the nondominated solution based on the parallel cell entropy is proposed. A new generated solution is compared with the archive to verify if it dominates any member of the archive. PAEA is shown in detail in Algorithm 1.

D. Evolutionary Status

By calculating the entropy ratio, we can estimate the evolutionary status of the bacterial populations. Inspired by the literature [38], three evolutionary statuses are defined as follows.

1) Convergence Status: Convergence status describes that the approximate Pareto front obtained is approaching the true Pareto one. This status may occur in two cases. One case is that the archive is not filled; the other is that the archive still has space to accommodate a new solution after these dominated old solutions are removed from the archive because the new solution obtained is not dominated by any old solution in the archive, instead, the new solution dominates one or more old solutions.

2) Diversity Status: When the number of the approximate Pareto front has reached the maximum capacity of the archive and the new solution and all members of the archive are nondominant solution for each other, the obtained new solution replaces the older solution with larger individual density in the archive to enhance diversity of the approximate Pareto front. We call this case as diversity status.

3) Stagnation Status: It describes that the approximate Pareto front is not changed between the tth and the $(t-1)$th populations because the new solution is rejected and is not added in the archive. The reasons for this may be listed as follows: new solution is dominated by any old solution in the archive; new solution has larger individual density than any old solution in the archive.

Let K be the maximum capacity of the archive and M the number of members in the archive, we can acquire the critical threshold δ_c on the convergence status by

$$\delta_c = \frac{2}{H} \log 2. \tag{15}$$

Similarly, the critical threshold δ_s of the stagnation status is introduced by

$$\delta_s = \frac{2}{MK} \log 2. \tag{16}$$

According to the analysis of the literature [40], there are several determinant conditions of the evolutionary status as listed below.

1) The tth population is on the convergence status if $|\Delta E(t)| > \delta_c$ or $|H(t) - H(t-1)| > 0$.
2) The tth population is on the diversity status if $\delta_s < |\Delta E(t)| < \delta_c$ and $H(t) = H(t-1) = K$.
3) The tth population is on the stagnation status if $|\Delta E(t)| < \delta_s$ and $H(t) = H(t-1)$.

E. Adaptive Foraging Strategy

In the classic BFO, the chemotactic movement of a bacterium is the major driving force. It can be updated as follows:

$$\theta^i(j+1,k,l) = \theta^i(j,k,l) + C_t(i) \frac{\Delta(i)}{\sqrt{\Delta^T(i)\,\Delta(i)}} \tag{17}$$

where $\theta^i(j,k,l)$ is the location of the ith bacterium in the tth generation at jth chemotactic, kth reproductive, and lth elimination dispersal step. $\Delta(i)$ represents a vector in the random direction whose elements lie in $[-1,1]$. $C_t(i)$ indicates the size of the step taken in the random direction specified by the tumble, and it can be used to control each individual who can dynamically transform between the exploit and the explore state to adjust the diversity and convergence of the population. Generally speaking, the individual will precisely exploit the neighborhood region to obtain the optimal solution with the smaller step size. Once the search process is completed or the local optimal solution is found, the individual will quickly leave the region with the larger chemotactic step and begin to do next exploration at a new area. Using the AFS, the population can evolve to satisfy the ultimate requirements.

Based on the above analysis, the adaptive adjustment strategy can be designed. When the tth population is determined on a different status, the adaptive chemotaxis step $C_t(i)$ is given as

$$C_t(i) = \begin{cases} C_{t-1}(i) - \lambda(1 + |\Delta E(t)|), & \text{if convergence} \\ C_{t-1}(i) + \mu|\Delta E(t)|, & \text{if diversity} \\ C_{t-1}(i), & \text{if stagnation} \end{cases} \tag{18}$$

where λ and μ are the adjustment step sizes.

From (18), $C_t(i)$ is not less than the certain value to effectively prevent the population from premature convergence and to increase the ability of escaping from a local minimum. Conversely, the convergence rate will reduce if $C_t(i)$ is too large. In this case, the algorithm may skip the optimal solution located in a narrow valley, and then the opportunity to find the optimal solution will be lost.

F. MOBFO Algorithm

In the classical BFO algorithm, bacterium always swims to a better region and runs away from dangerous places, or it tumbles to get ample amount of nutrient substance. For multi-objective problems, the value of the multipleobjective functions represents the gradient of nutrients in that location. To apply the BFO algorithm in solving MOPs, PAEA and AFS are applied to balance convergence and diversity of the Pareto front. The whole algorithm is shown in detail in Algorithm 2.

Algorithm 2. MOBFO

Input: multi-objective optimization problem MOP.
Output: approximate optimal solutions in the archive A.
t=0
$A = \emptyset$
for $i = 1 : S$ **do**
  calculate θ^i and J_m.
  update A using Algorithm 1.
end for
while $t < T_{\max}$ **do**
  $t \leftarrow t + 1$.
  map A onto PCCS.
  calculate $E(t)$ and $\Delta E(t)$.
  evaluate evolution status.
  calculate adaptive chemotaxis step by Eq.18.
  for $l = 1 : N_{ed}$ **do**
    for $k = 1 : N_{re}$ **do**
      for $j = j : N_c$ **do**
        for $i = 1 : S$ **do**
          update $\theta^i(j+1, k, l)$.
          calculate $J_m(i, j+1, k, l)$.
          update A using Algorithm 1.
        end for
      end for
      calculate $J_{health} = \sum_{j=1}^{N_c+1} J_m(i, j+1, k, l)$.
      select S_r bacterium with the highest J_{health} values to die, and the other non-dominated bacteria reproduce.
    end for
    According to low probability P_{ed}, some bacteria would be eliminated and moved to another position in the rich-food environment.
  end for
end while

IV. Experiments and Discussion

To measure the performance of the MOBFO algorithm, we select five classic MOO algorithms, 1) NSGA-II; 2) SPEA2; 3) MOEA/D; 4) MBFO; and 5) MOPSO, to compare with MOBFO, especially, on the convergence and the diversity performance of the Pareto front. In this section, our experiments fall into two parts. In the first part, ZDT1, ZDT2, ZDT3, ZDT4 [42], DTLZ1, and DTLZ2 benchmark problems [43] are utilized to examine the performance of the proposed method. Here, all benchmarks are run with default settings. Additionally, we use the example of the aluminum electrolysis production process to show the effect of choosing different solutions. The results below are achieved using MATLAB 2013a on a desktop computer (2.60GHz Intel Core i5, 4GB of RAM).

A. Performance Evaluation

The metric of generational distance (GD) [44] and spacing (S) [45], which can show the ability to attain the Pareto optimal set and the diversity distribution of the Pareto solutions, are often used to provide a quantitative assessment of the performance of multi-objective solvers.

B. Numerical Results and Analysis of Benchmarks

The obtained nondominated solutions by five well-known versions of the MOO and MOBFO for the benchmarks, in one arbitrary run, are shown in Tables I–IV and Figs. 3 and 4. When solving them, the population size is set at 100, and the maximum iteration is also set at 100. Each algorithm has been executed in 30 independent runs.

Table I, which is limited by the number of pages, only shows the optimal Pareto front obtained by the proposed algorithms for ZDT1-4, and DTLZ1-2 problems. The performances of these compared algorithms are so close that they achieve the best extent of spread among the optimal solutions found for ZDT1, ZDT2, and ZDT3. However, for ZDT4, graphical results become very different. The solutions generated by MOBFO are well distributed and cover the entire Pareto front of the problem, and it is slightly below the MOEA/D and MBFO with respect to the error ratio, whereas NSGA-II is not able to cover the entire Pareto front of the problem. For many-objective problems, especially DTLZ1 and DTLZ2, the diversity of the Pareto front gained is significantly better than that of other algorithms due to the application of PAEA, which is a technique to update the archive of the nondominated solution to maintain population diversity. It suggests that the method of mapping the Pareto front onto PCCS may be more suitable in helping optimization algorithms solve the many-objective optimization problems.

Table II shows the comparison of results among six algorithms considering the previously described metric GD. It can

TABLE I
PARETO FRONTS OF COMPARISON ALGORITHMS ON THREE TEST INSTANCES

ZDT1 ZDT2 ZDT3

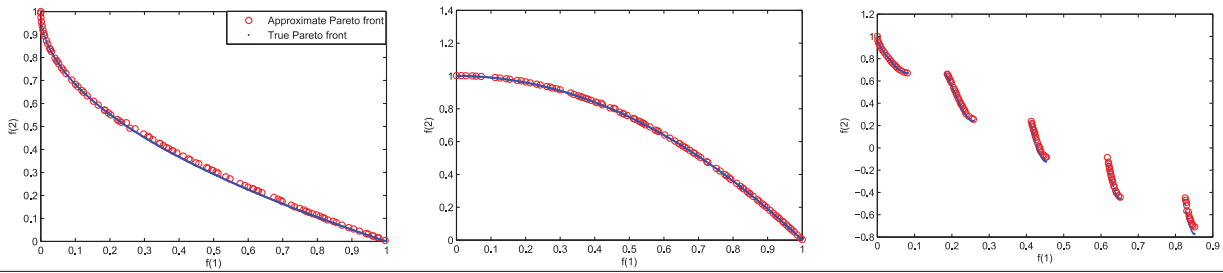

ZDT4 DTLZ1 DTLZ2

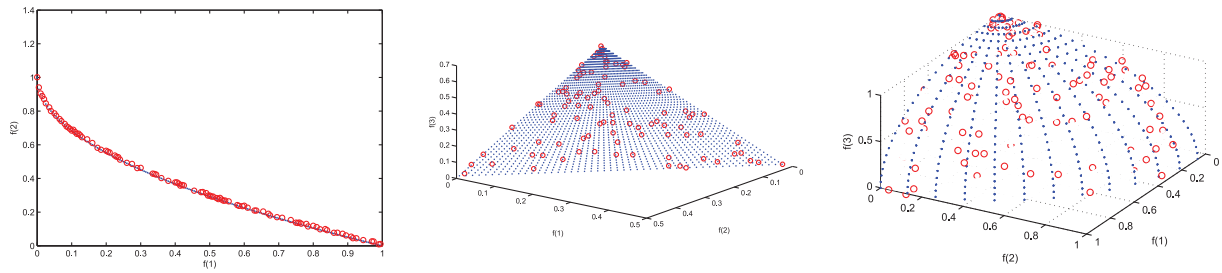

(For table 1, blue dot is true Pareto front while red circle is approximate Pareto front.)

TABLE II
RESULTS OF THE METRICS GD AND S

Problem		NSGA-II		SPEA2		MOPSO		MOEA/D		MBFO		MOBFO	
		GD	S	GD	S	GD	S	GD	S	GD	S	GD	S
ZDT1 (e-3)	Best	7.962	39.77	8.109	40.16	8.101	40.95	8.192	38.98	9.463	37.82	8.276	41.26
	Mean	8.345	41.34	8.450	42.06	8.461	42.50	8.667	42.82	11.15	40.75	8.501	42.18
	Std. Dev.	0.235	2.451	0.167	3.369	0.236	3.669	0.286	5.747	1.990	6.084	0.135	2.259
ZDT2 (e-3)	Best	8.172	39.22	8.111	39.55	8.253	40.19	8.155	38.55	8.479	37.97	8.147	31.47
	Mean	9.321	44.52	8.958	42.12	9.226	43.09	8.321	42.27	10.54	42.56	8.302	33.58
	Std. Dev.	1.786	15.52	1.787	14.01	1.708	19.36	0.181	19.97	2.092	17.41	0.147	3.292
ZDT3 (e-3)	Best	11.43	36.67	11.88	42.67	12.25	33.78	11.01	31.84	13.48	33.66	11.33	37.18
	Mean	12.66	50.02	12.71	51.47	13.47	51.51	13.68	48.30	14.93	45.39	11.73	39.44
	Std. Dev.	0.911	7.761	0.764	7.005	1.323	9.681	1.416	11.59	1.005	8.834	0.222	1.646
ZDT4 (e-3)	Best	13.31	45.96	12.23	45.42	13.32	45.41	12.97	42.43	12.89	44.39	12.14	42.65
	Mean	14.40	60.92	13.71	53.12	15.02	57.15	14.87	51.46	15.14	48.84	12.89	45.10
	Std. Dev.	1.068	16.33	2.087	8.342	1.638	19.42	1.465	12.15	1.854	5.544	0.689	4.006
DTLZ1 (e-2)	Best	19.60	13.82	20.92	14.92	16.67	14.69	20.26	16.99	20.49	14.24	13.02	12.78
	Mean	32.69	18.15	35.09	19.56	19.54	19.20	33.46	20.64	33.42	22.26	14.84	15.59
	Std. Dev.	11.22	5.754	9.954	5.867	2.038	6.772	11.29	5.023	8.245	10.13	2.591	4.326
DTLZ2 (e-2)	Best	10.65	33.53	10.37	31.48	14.01	32.98	11.28	34.89	10.63	33.42	8.048	30.18
	Mean	14.43	39.41	13.94	35.81	16.67	36.64	16.41	36.68	15.95	35.71	10.44	31.95
	Std. Dev.	2.895	7.259	3.152	6.363	2.937	6.563	3.645	3.429	3.523	3.830	1.514	3.364

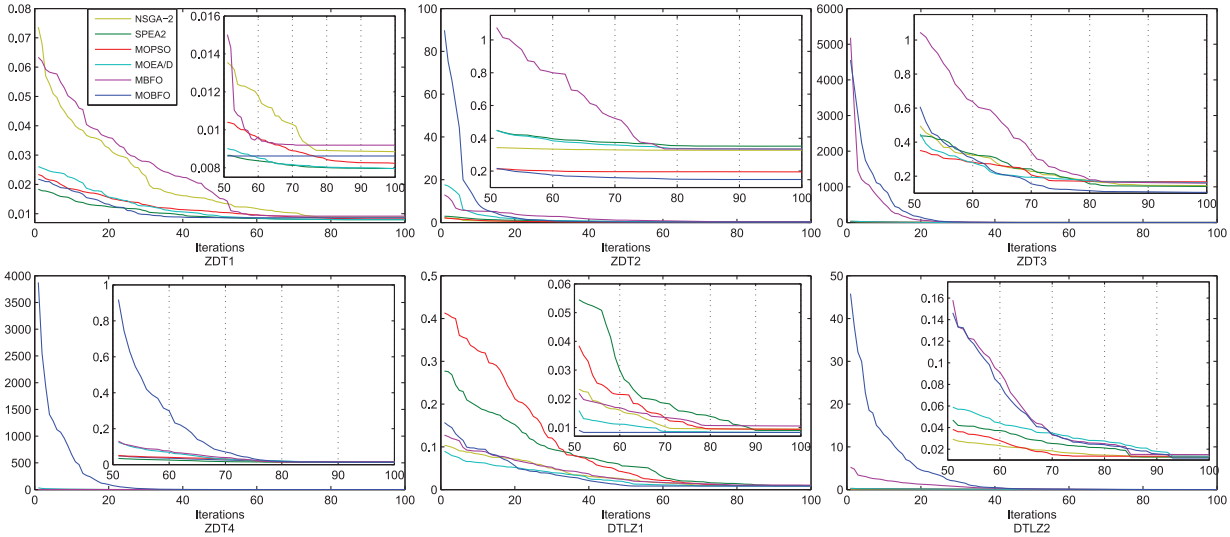

Fig. 3. Convergence comparison in terms of the metric GD. The number of iterations required to achieve convergence is estimated by six algorithms in the scope of 100 iterations. (Inset) The trend of convergence is described from the 50th generation to the 100th generation to show the details.

be seen that the average performance of MOBFO is the best with respect to test problems. For instance, MOBFO places slightly below the SPEA2 on the best solution for ZDT2, but with a lower mean and standard deviation of the metric GD, which can better reflect the distance between the solutions and the true Pareto front. It is worth noting that the performance of MOBFO is far superior to that of MBFO, though the two algorithms are both MOO based on BFO. It denotes that the parallel coordinate has excellent mapping ability from high-dimensional Pareto front to a two-dimensional space, then the Pareto optimal solution set can be indirectly and rapidly evaluated. Table II also lists the comparison of results of the test algorithms considering the previously described metric S. It is shown that MOBFO has stale and good diversity with the corresponding metric S always kept at high value, especially in the DTLZ1 and DTLZ2 problems. This indicates that the application of MOBFO is successful in maintaining diversity of the Pareto front for many-objective problems. The results show that the proposed algorithm performs better than the other algorithms on the diversity of the Pareto solutions. It suggests that determinant conditions of the evolutionary status based on parallel cell entropy and its difference are reasonable. To obtain the appropriate step sizes λ and μ, a large number of experiments and attempts seem necessary.

To investigate the computational cost of the proposed algorithm, we define the effective convergence time.

Effective convergence time: It is the time spent by the evolution algorithm from the beginning of iteration to convergence and the point of termination of searching solutions, which is the product of the number of iterations required to convergence N_{it} and the time needed for each iteration T_{it}

$$T_{\text{EC}} = N_{\text{it}} \cdot T_{\text{it}} \tag{19}$$

where T_{EC} is the effective convergence time. In fact, the value of N_{it} is not constant in each optimization due to the property of swarm intelligence computing.

The value of N_{it} should be taken as the maximum of $N_{\text{it}}(i)$ for N independent tests to make sure that the algorithm can converge in each test. N_{it} can be expressed as follows:

$$N_{\text{it}} = \max_{i\in(1,n)} \{N_{\text{it}}(i)\} = \max_{i\in(1,n)} \{\max\{N_{\text{it,GD}}(i), N_{\text{it},S}(i)\}\} \tag{20}$$

where $N_{\text{it,GD}}(i)$ and $N_{\text{it},S}(i)$ are the numbers of iteration required to achieve convergence of the GD and the S in the ith independent test, respectively. The larger number of iteration $N_{\text{it}}(i)$ is chosen between $N_{\text{it,GD}}(i)$ and $N_{\text{it},S}(i)$ to guarantee that both the GD and the S can be converged in the evolution process.

By combining (19) and (20), we have

$$T_{\text{EC}} = T_{\text{it}} \cdot \max_{i\in(1,n)} \{\max\{N_{\text{it,GD}}(i), N_{\text{it},S}(i)\}\}. \tag{21}$$

The effective convergence time is characterized by the computational cost of the evolutionary algorithm. It is obvious that the smaller the effective convergence time is, the smaller the time cost of the evolutionary algorithm is. We select the maximum of $N_{\text{it}}(i)$ for every algorithm from 30 independent tests to compare the effective convergence time in terms of six benchmarks.

As shown in Figs. 3 and 4, the proposed MOBFO converges significantly faster than the other classical MOO algorithms. To analyze further, the number of iterations to convergence is shown in Table III.

The convergence speed of an algorithm is closely correlated to the initial population. Specifically, achieving convergence for the algorithm is difficult if the initial values of GD and S are large. However, MOBFO can still get satisfactory convergence performance, especially in the ZDT2, ZDT3, ZDT4, and DTLZ2 problems.

Table IV lists the average times needed for each iteration. We can observe that MOBFO needed more time than the other algorithms. The main reason for this is that the main body of

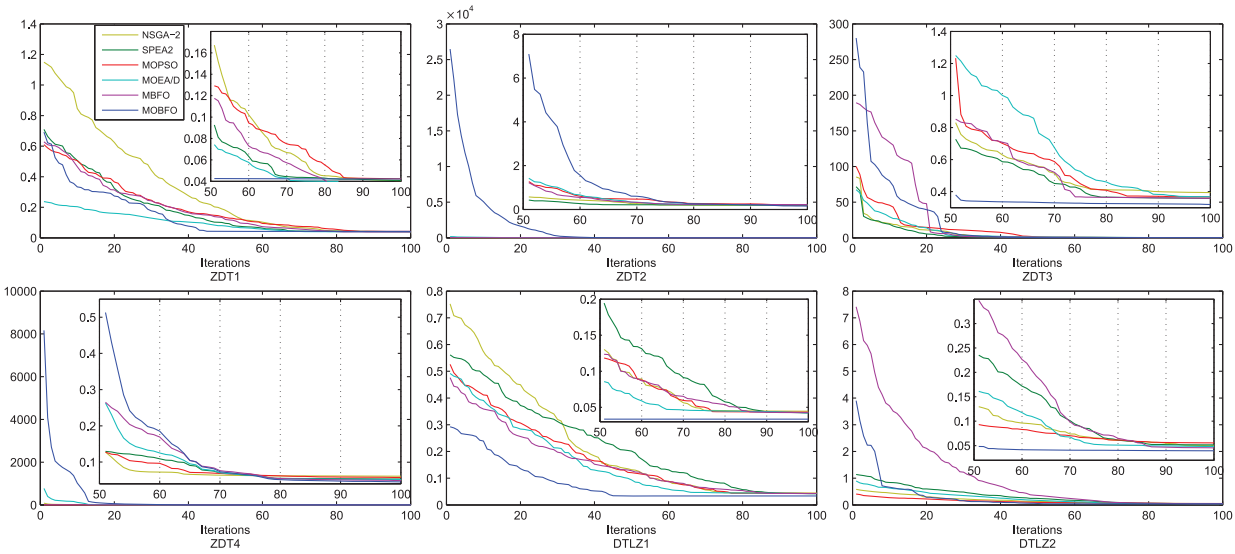

Fig. 4. Convergence comparison in terms of the metric S.

TABLE III
NUMBER OF ITERATIONS REQUIRED FOR CONVERGENCE

Problem	NSGA-II		SPEA2		MOPSO	
	GD	S	GD	S	GD	S
ZDT1	83	89	86	72	89	85
ZDT2	75	79	79	64	60	82
ZDT3	70	62	80	70	72	67
ZDT4	81	40	78	80	80	85
DTLZ1	71	75	89	86	79	77
DTLZ2	88	92	85	87	73	89
	MOEA/D		MBFO		MOBFO	
	GD	S	GD	S	GD	S
ZDT1	87	78	71	81	50	45
ZDT2	68	61	78	71	45	37
ZDT3	62	81	31	67	31	41
ZDT4	52	36	78	78	32	29
DTLZ1	80	66	79	84	52	45
DTLZ2	92	78	84	75	72	51

MOBFO is a three-layer loop of nested structure, which leads to a large time overhead. In addition, the introduction of the PEAE and AFS strategy increases the computational cost of the inner loop of the MOBFO, and further increases the time consumed for each iteration.

The comparison results about effective convergence time are also summarized in Table IV. It can be seen from Table IV that the time spent by MOBFO from the beginning of the iteration to the point of stopping of searching solutions is obviously faster than those of other algorithms, which benefits from the design of PEAE and AFS.

TABLE IV
AVERAGE TIME NEEDED FOR EACH ITERATION [EFFECTIVE CONVERGENCE TIME (S)]

Problem	NSGA-II	SPEA2	MOPSO
ZDT1	1.24 (110.36)	2.26 (194.36)	1.29 (114.81)
ZDT2	2.05 (166.05)	1.37 (109.60)	2.25 (191.25)
ZDT3	1.57 (124.03)	1.36 (107.44)	1.44 (118.08)
ZDT4	1.85 (129.50)	1.77 (141.6)	1.57 (113.04)
DTLZ1	2.95 (221.25)	2.39 (212.71)	2.65 (209.35)
DTLZ2	2.89 (265.88)	2.54 (220.98)	2.66 (236.74)
	MOEA/D	MBFO	MOBFO
ZDT1	1.33 (115.71)	1.28 (103.68)	2.03 (101.5)
ZDT2	1.72 (89.44)	2.09 (163.02)	2.12 (67.84)
ZDT3	1.37 (93.16)	1.48 (115.44)	1.65 (74.25)
ZDT4	2.08 (168.48)	1.79 (119.93)	2.32 (95.12)
DTLZ1	2.61 (208.80)	2.58 (216.72)	3.17 (164.84)
DTLZ2	2.63 (241.96)	2.64 (221.76)	3.02 (217.44)

(a) (b)

Fig. 5. 170KA series of aluminum reduction cell as the test bench [3], [46] (a) Allotype cathode. (b) Perforation anode.

TABLE V
PARAMETER SETTINGS OF BPNN

Objective function	V_{CF_4}	CE	W
Iteration	800	800	800
Transfer function in hidden layer	Tansig	Logsig	Tansig
Transfer function in output layer	Purelin	Purelin	Purelin
Hidden nodes	13	12	13

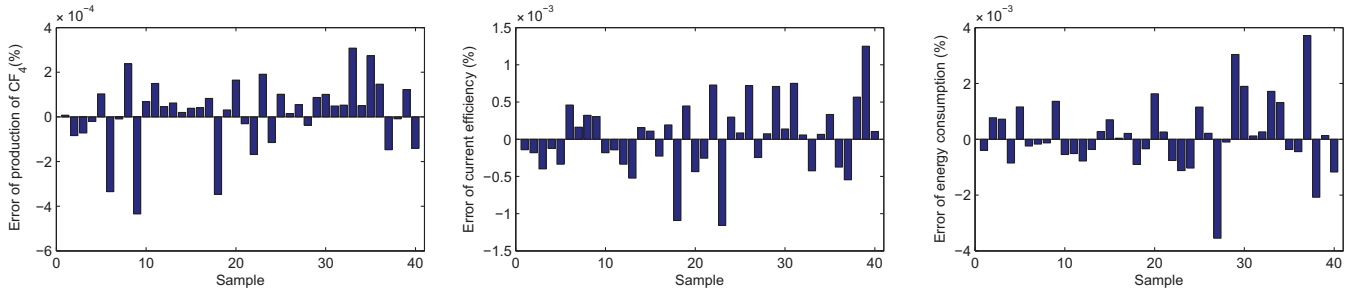

Fig. 6. Predicted error for the objective function models. Predicted error of (a) production of CF_4; (b) current efficiency; and (c) energy consumption.

TABLE VI
PART OF THE PARETO SOLUTIONS

	V_{CF_4} (kg)	CE (%)	W (kWh/t-Al)	x_1 (A)	x_2	x_3 (%)	x_4 (kg)	x_5 (cm)	x_6 (cm)	x_7 (°C)	x_8 (mV)
	3.85	97.81	11 093.12	1685	610	2.47	1210	16	14	930	3641
NSGA-II	3.90	94.75	11 432.51	1664	615	2.46	1210	17	14.5	947	3635
	3.75	98.89	10 938.82	1680	610	2.35	1280	16.5	14	930	3630
	3.85	95.55	11 358.62	1688	632	2.40	1180	16	15	935	3642
SPEA2	3.98	97.59	11 087.59	1698	618	2.37	1210	17	14.5	960	3631
	3.58	98.75	10 915.10	1689	628	2.45	1280	17.5	15.5	930	3617
	3.75	98.98	10 974.04	1679	631	2.45	1220	16	14	940	3645
MOPSO	3.78	97.13	11 327.25	1673	626	2.39	1100	17	15	944	3692
	3.90	94.37	11 478.54	1680	610	2.47	1080	17.5	15.5	930	3635
	3.80	94.05	11 457.40	1701	638	2.43	1160	16	15	950	3616
MOEA/D	3.43	93.85	11 526.27	1681	660	2.47	1250	14.5	16	945	3630
	4.04	97.85	11 055.08	1679	659	2.53	1270	17	14	938	3630
	3.95	95.54	11 322.38	1679	626	2.48	1240	18.5	17	945	3630
MBFO	4.14	97.08	11 182.67	1696	632	2.43	1260	17	15	955	3643
	3.99	93.98	11 700.57	1687	623	2.45	1190	16	15	951	3690
	3.70	97.80	11 030.27	1701	622	2.48	1270	17	17	938	3620
MOBFO	3.79	98.38	10 995.53	1689	616	2.49	1270	16.5	16	944	3630
	3.72	97.97	11 056.75	1695	620	2.43	1280	17.5	16	935	3635

The parallel cell entropy is used as a means of evaluating the distribution of the Pareto front, and then the performance of the solutions obtained is evaluated to update the archive in PEAE. Using PEAE, the elite individual can be better retained, so as to drive the bacteria to move in the best direction to achieve the goal of rapid convergence.

In the original BFO algorithm, the chemotactic operation is the main body, and an accurate chemotactic step size plays a key role on diversity and convergence of the populations. But the application of the constant step size easily leads to slowing down of the convergence speed and to the occurrence of the phenomenon of premature appearance. With the introduction of AFS, the chemotactic step size can be adaptively adjusted according to the evolution status. This strategy can be a good way to avoid the shortcomings of the constant step size.

C. Results and Analysis of the Aluminum Electrolysis Production Process

In this section, we selected 365 sets of daily data in the full year of 2013 to develop an objective function model, and 40 sets from January 1, 2014 to February 31, 2014 were selected to test the accuracy of a predictive model. The 170KA series of the aluminum reduction cell of Chongqing Tiantai Aluminum Corporation Ltd., which is a new electrolytic equipment combined with two energy-saving technologies (allotype

cathode and perforated anode), is shown as the test platform in Fig. 5.

Based on the MOO framework, eight kinds of variables are selected as follows: 1) the current series (x_1); 2) the blanking times (x_2); 3) the molecular ratio (x_3); 4) the amount of aluminum (x_4); 5) the aluminum level (x_5); 6) the electrolyte level (x_6); 7) the bath temperature (x_7); and 8) the cell voltage (x_8) with the nonlinear feature selection method. As the second step of this framework, the back propagation artificial neural network (BPNN) is used to satisfy the higher accuracy requirement of an objective function modelling, which greatly affects the achievement of optimized performance. The detailed parameter settings of the model are summarized in Table V.

After the training process of BPNN, the predicted results of the three objective function models are achieved, as shown in Fig. 6. The maximum predicted error of the production of CF_4 and the current efficiency and energy consumptions are 2.3%, -3%, and -4.9%, respectively. Considering the complexity of modeling, the predicted accuracy is enough to meet the next MOO requirements.

To validate MOBFO for the aluminum electrolysis production process, optimal results about the three objective functions are given between the production data and the six algorithms for comparison purposes. As shown in Table VI, production data are the average values of the real output in 2014, whereas other optimal results represent one of the Pareto solutions grouped using several algorithms. It is clearly observed that MOBFO can achieve the best preference in terms of the three objective functions by introducing parallel cell entropy into the BFO.

Three groups of the Pareto solutions are selected to compare the performance of the optimization algorithms in Table VI. A similar conclusion is found. For instance, after using MOBFO, in one hand, the energy consumption is only 11 030.27 kWh / t-Al, which means the dc power consumption is reduced dramatically. On the other hand, CF_4 emissions can be decreased to 3.70 kg in one day. It is worth noting that the corresponding voltage must be reduced to 3620 mV while maintaining steady status. This requires the application of effective production management measures and energy-saving technologies.

V. Conclusion

In this paper, we have proposed MOBFO, an improved MOO algorithm based on BFO algorithm, to solve the MOPs in the aluminum electrolysis production process. The formulas of the multiple objective functions can be determined using the maximum of the current efficiency and the minimum of the energy consumption and the minimum of the production of PFC. To rapidly evaluate the Pareto solution sets and to reduce the amount of calculation, concepts of the Pareto entropy are developed in PCCS. In addition, the PAEA and the adaptive scheme have been designed to maintain diversity of the Pareto front and to obtain better convergence of the algorithm. The experimental comparison results of MOBFO with other five algorithms show the effectiveness of the proposed approach in six different benchmark problems and in the real test platform. This suggests that the proposed method may be more suited in solving the high-dimensional many-objective optimization problem. Future works should further evaluate the performance of new algorithms to solve optimization problems with more than three objectives.

References

[1] U. Grjotheim and H. Kvande, *Introduction to Aluminium Electrolysis. Understanding the Hall-Heroult Process*. Dusseldorf, Germany: Aluminium Verlag GmbH, 1993.

[2] T. Li, L. Yao, J. Yi, W. Hu, Y. Su, and W. Jia, "An improved UKFNN based on square root filter and strong tracking filter for dynamic evolutionary modeling of aluminum reduction cell," *Acta Autom. Sin.*, vol. 40, no. 3, pp. 522–530, Mar. 2014.

[3] N. Feng, Y. Tian, J. Peng, Y. Wang, X. Qi, and G. Tu, "New cathodes in aluminum reduction cells," in *Proc. TMS Annu. Meeting Exhib.*, Seattle, WA, USA, Feb. 2010, pp. 523–526.

[4] Y. Tian, N. Feng, J. Peng, Y. Wang, and J. Li, "The combined flame and aluminum preheating method," in *Proc. TMS Annu. Meeting Exhib.*, Seattle, WA, USA, Feb. 2010, pp. 613–616.

[5] S. Zeng, S. Wang, and Y. Qu, "Control of temperature and aluminum fluoride concentration based on model prediction in aluminum electrolysis," *Adv. Mater. Sci. Eng.*, vol. 2014, p. 5, 2014.

[6] A. Chaouachi, R. M. Kamel, R. Andoulsi, and K. Nagasaka, "Multiobjective intelligent energy management for a microgrid," *IEEE Trans. Ind. Electron.*, vol. 60, no. 4, pp. 1688–1699, Apr. 2013.

[7] K. Deb, *Multi-Objective Optimisation Using Evolutionary Algorithms: An Introduction*. New York, NY, USA: Springer, 2011.

[8] A. F. Zobaa, "Optimal multi-objective design of hybrid active power filters considering a distorted environment," *IEEE Trans. Ind. Electron.*, vol. 61, no. 1, pp. 107–114, Jan. 2014.

[9] R. B. Godoy, J. O. P. Pinto, C. A. Canesin, and E. Coelho, "Differential-evolution-based optimization of the dynamic response for parallel operation of inverters with no controller interconnection," *IEEE Trans. Ind. Electron.*, vol. 59, no. 7, pp. 2859–2866, Jul. 2012.

[10] Q. Zhang and H. Li, "MOEA/D: A multi-objective evolutionary algorithm based on decomposition," *IEEE Trans. Evol. Comput.*, vol. 11, no. 6, pp. 712–731, Dec. 2007.

[11] E. Zitzler and L. Thiele, "Multi-Objective evolutionary algorithms: A comparative case study and the strength Pareto approach," *IEEE Trans. Evol. Comput.*, vol. 3, no. 4, pp. 257–271, Nov. 1999.

[12] E. Zitzler, M. Laumanns, and L. Thiele, "SPEA2: Improving the strength Pareto evolutionary algorithm," K. Giannakoglou, D. T. Tsahalis, J. Priaux, K. D. Papailiou, and T. Fogarty, Eds. Berlin, Germany: Springer-Verlag, 2002, pp. 95–100.

[13] J. D. Knowles and D. W. Corne, "Approximating the nondominated front using the Pareto archived evolution strategy," *Evol. Comput.*, vol. 8, no. 2, pp. 149–172, 2000.

[14] D. W. Corne, J. D. Knowles, and M. J. Oates, *The Pareto Envelope-Based Selection Algorithm for Multi-Objective Optimization*. Berlin, Germany: Springer-Verlag, 2000, vol. 1917, pp. 869–878.

[15] D. W. Corne, N. R. Jerram, and J. D. Knowles, "PESA-II: Region-based selection in evolutionary multi-objective optimization," in *Proc. Genet. Evol. Comput. Conf. (GECCO'01)*, 2001, pp. 283–290.

[16] C. Coello and G. Pulido, "A micro-genetic algorithm for multi-objective optimization," in *Proc. Genet. Evol. Comput. Conf. (GECCO'01)*, 2001, pp. 274–282.

[17] K. Deb, A. Pratap, S. Agarwal, and T. Meyarivan, "A fast and elitist multiobjective genetic algorithm: NSGA-II," *IEEE Trans. Evol. Comput.*, vol. 6, no. 2, pp. 182–197, Apr. 2002.

[18] Z. Gao and D. Zhang, "Performance analysis, mapping, and multiobjective optimization of a hybrid robotic machine tool," *IEEE Trans. Ind. Electron.*, vol. 62, no. 1, pp. 423–433, Jan. 2015.

[19] K. Deb, "Multi-objective optimization," in *Search Methodologies*. New York, NY, USA: Springer, 2014, vol. 403–449.

[20] S. C. Wang and Y. H. Liu, "A PSO-based fuzzy-controlled searching for the optimal charge pattern of Li-Ion batteries," *IEEE Trans. Ind. Electron.*, vol. 62, no. 5, pp. 2983–2993, May 2015.

[21] Q. Li, W. Chen, Y. Wang, S. Liu, and J. Jia, "Parameter identification for PEM fuel-cell mechanism model based on effective informed adaptive particle swarm optimization," *IEEE Trans. Ind. Electron.*, vol. 58, no. 6, pp. 2410–2419, Jun. 2011.

[22] C. Coello, G. Pulido, and M. Lechuga, "Handing multiple objectives with particle swarm optimization," *IEEE Trans. Evol. Comput.*, vol. 8, no. 3, pp. 256–279, Jun. 2004.

[23] M. Gong *et al.*, "Multi-objective immune algorithm with nondominated neighbor-based selection," *Evol. Comput.*, vol. 16, no. 2, pp. 225–255, 2008.
[24] Q. Zhang, A. Zhou, and Y. Jin, "RM-MEDA: A regularity model-based multi-objective estimation of distribution algorithm," *IEEE Trans. Evol. Comput.*, vol. 12, no. 1, pp. 41–63, Feb. 2008.
[25] M. Shen, Z. Zhan, W. N. Chen, Y. J. Gong, J. Zhang, and Y. Li, "Bi-velocity discrete particle swarm optimization and its application to multicast routing problem in communication networks," *IEEE Trans. Ind. Electron.*, vol. 61, no. 12, pp. 7141–7151, Dec. 2014.
[26] Y. Zhang, Y. Yang, S. X. Ding, and L. Li, "Data-driven design and optimization of feedback control systems for industrial applications," *IEEE Trans. Ind. Electron.*, vol. 61, no. 11, pp. 6409–6417, Nov. 2014.
[27] A. Karaarsian, "The implementation of bee colony optimization algorithm to Sheppard–Taylor PFC converter," *IEEE Trans. Ind. Electron.*, vol. 60, no. 9, pp. 3711–3719, Sep. 2013.
[28] J. Guo, W. Gui, and X. Wen, "Multi-objective optimization for aluminum electrolysis production process," *J. Central South Univ. China*, vol. 43, no. 2, pp. 548–553, 2012.
[29] J. Guo, W. Gui, and C. Yang, "An improved hybrid differential evolution algorithm used for multi-objective optimization of aluminum electrolysis," *J. Central South Univ. China*, vol. 43, no. 1, pp. 184–188, 2012.
[30] K. M. Passino, "Biomimicry of bacterial foraging for distributed optimization and control," *IEEE Control Syst. Mag.*, vol. 22, no. 3, pp. 52–67, Jun. 2002.
[31] Y. Liu and K. Passino, "Biomimicry of social foraging bacteria for distributed optimization: Models, principles, and emergent behaviors," *J. Optim. Theory Appl.*, vol. 115, no. 3, pp. 603–628, 2002.
[32] S. Yin and Z. Huang, "Performance monitoring for vehicle suspension system via fuzzy positivistic C-means clustering based on accelerometer measurements," *IEEE/ASME Trans. Mechatronics*, vol. 20, no. 5, pp. 2613–2620, Oct. 2015.
[33] S. Yin, X. Zhu, and O. Kaynak, "Improved PLS focused on key-performance-indicator-related fault diagnosis," *IEEE Trans. Ind. Electron.*, vol. 62, no. 3, pp. 1651–1658, Mar. 2015.
[34] S. Yin, S. Ding, X. Xie, and H. Luo, "A review on basic data-driven approaches for industrial process monitoring," *IEEE Trans. Ind. Electron.*, vol. 61, no. 11, pp. 6418–6428, Nov. 2014.
[35] T. Li, J. Yi, Y. Su, W. Hu, and T. Gao, "Variable selection for nonlinear modeling based on false nearest neighbours in KPCA subspace," *J. Mech. Eng.*, vol. 48, no. 10, pp. 192–198, 2012.
[36] T. Kuroki *et al.*, "CF4 decomposition using inductively coupled plasma: Effect of power frequency," *IEEE Trans. Ind. Appl.*, vol. 41, no. 1, pp. 215–220, Jan./Feb. 2005.
[37] A. Tabereaux, "Anode effects, PFCs, global warming, and the aluminum industry," *JOM*, vol. 46, no. 11, pp. 30–34, 1994.
[38] W. Hu, G. G. Yen, and X. Zhang, "Multi-objective particle swarm optimization based on Pareto entropy," *J. Softw.*, vol. 25, no. 5, pp. 1025–1050, 2014.
[39] A. Inselberg, "The plane with parallel coordinates," *Visual Comput.*, vol. 1, no. 2, pp. 69–91, 1985.
[40] B. K. Panigrahi *et al.*, "Multi-objective bacteria foraging algorithm for electrical load dispatch problem," *Energy Convers. Manage.*, vol. 52, no. 2, pp. 1334–1342, 2011.
[41] M. A. Guzmn, A. Delgado, and J. D. Carvalho, "A novel multi-objective optimization algorithm based on bacterial chemotaxis," *Eng. Appl. Artif. Intell.*, vol. 23, no. 3, pp. 292–301, 2010.
[42] K. Deb, L. Thiele, M. Laumanns, and E. Zitzler, "Scalable multi-objective optimization test problems," in *Proc. IEEE Congr. Evol. Comput. (CEC'02)*, 2002, pp. 825–830.
[43] S. Mostaghim and J. Teich, "Strategies for finding good local guides in multi-objective particle swarm optimization (MOPSO)," in *Proc. IEEE Swarm Intell. Symp. (SIS'03)*, 2003, pp. 26–33.
[44] K. Deb and S. Jain, "Running performance metrics for evolutionary multi-objective optimization," Indian Inst. Technol., Kanpur, India, Tech. Rep. 2002004, 2002.
[45] J. R. Schott, "Fault tolerant design using single and multicriteria genetic algorithm optimization," M.S. thesis, Dept. Aeronaut. Astronaut., Massachusetts Inst. Technol., Cambridge, MA, USA, 1995.
[46] Y. Tian and H. Wang, "Study of ACD model and energy consumption in aluminum reduction cells," in *Proc. TMS Annu. Meeting Exhib.*, San Diego, CA, USA, Feb. 2011, pp. 567–568.

Jun Yi received the B.S. and M.S. degrees in computer science and technology from the University of Electronic Science and Technology of China, Chengdu, China, in 2002 and 2006, respectively, and the Ph.D. degree in control theory and engineering from Chongqing University, Chongqing, China, in 2010.

He is currently an Associate Professor with the College of Electrical and Information Engineering, Chongqing University of Science and Technology, Chongqing, China. His research interests include industrial process modeling and intelligent optimization.

Di Huang received the B.S. degree in metallurgy engineering from Chongqing University of Science and Technology, Chongqing, China, where he is currently working toward the M.S. degree in the College of Electrical and Information Engineering.

Siyao Fu (M'08) received the Ph.D. degree in electrical engineering from the State Key Laboratory of Management and Control for Complex Systems, Institute of Automation, Chinese Academy of Sciences, Beijing, China, in 2008.

From September 2008 to December 2012, he was an Associate Professor with the Department of Electrical and Computer Engineering, Minzu University, Beijing, China. From January 2013 to July 2015, he was a Postdoctoral Research Fellow with the Department of Electrical, Computer, and Biomedical Engineering, University of Rhode Island, Kingston, RI, USA. He is currently a Lecturer with the Department of Computer Science, University of Massachusetts Boston, Boston, MA, USA. His research interests include computer vision, computational intelligence, machine learning, and data mining.

Haibo He (SM'11) received the B.S. and M.S. degrees from Huazhong University of Science and Technology, Wuhan, China, in 1999 and 2002, respectively, and the Ph.D. degree from Ohio University, Athens, OH, USA, in 2006, all in electrical engineering.

He is currently the Robert Hass Endowed Professor of Electrical Engineering with the University of Rhode Island, Kingston, RI, USA. From 2006 to 2009, he was an Assistant Professor with the Department of Electrical and Computer Engineering, Stevens Institute of Technology, Hoboken, NJ, USA. He has authored one sole-author research book (Wiley), edited one book (Wiley-IEEE) and six conference proceedings (Springer), and authored or coauthored over 180 peer-reviewed journal and conference papers. His research interests include computational intelligence, smart grid, cyber security, and various applications such as smart grid, cognitive radio, sensor networks, and others.

Dr. He is currently an Associate Editor of the IEEE TRANSACTIONS ON NEURAL NETWORKS AND LEARNING SYSTEMS, *IEEE Computational Intelligence Magazine*, and IEEE TRANSACTIONS ON SMART GRID. He was the recipient of the IEEE International Conference on Communications (ICC) Best Paper Award (2014), IEEE Computational Intelligence Society (CIS) Outstanding Early Career Award (2014), National Science Foundation (NSF) CAREER Award (2011), and Providence Business News (PBN) "Rising Star Innovator of The Year" Award (2011).

Taifu Li received the B.S., M.S., and Ph.D. degrees in mechanical engineering from Chongqing University, Chongqing, China, in 1996, 2000, and 2004, respectively.

He is currently a Professor with the College of Electrical and Information Engineering, Chongqing University of Science and Technology, Chongqing, China. His research interests include industrial process modeling and intelligent optimization.